Heliyon 10 (2024) e33067

Contents lists available at ScienceDirect

Heliyon

journal homepage: www.cell.com/heliyon

Research article

# Decelerating catalyst aging of natural gas engines using organic Rankine cycle under road conditions

Chongyao Wang [a], Xin Wang [a,*], Yunshan Ge [a], Yonghong Xu [b], Lijun Hao [a], Jianwei Tan [a], Ruonan Li [a], Miao Wen [a], Yachao Wang [a]

[a] School of Mechanical Engineering, Beijing Institute of Technology, Zhongguancun South Street No.5, 100081 Beijing, China
[b] Mechanical Electrical Engineering School, Beijing Information Science and Technology University, Xiaoying east road No.12, 100192 Beijing, China

ARTICLE INFO

*Keywords:*
NG engine
Waste heat recovery
Organic rankine cycle
Road condition
Three-way catalyst
Thermal aging

ABSTRACT

High exhaust temperature is an intrinsic nature of natural gas engines which underlies power de-rating and thermal aging of after-treatment system; therefore, this study integrates an organic Rankine cycle (ORC) system between engine and it's three-way catalyst (TWC) to address these challenges. ORC facilitates power output enhancement through exhaust energy recovery and alleviates thermal aging by reducing exhaust temperature. To estimate the effectiveness of this hypothesized system, a simulation-based investigation is performed. First, simulation models, including engine, TWC, and vehicle dynamic models, are built and validated by experimental data. According to the temperature characteristics of different TWCs, three scenarios, representing old, current, and prospective TWC technology, are formulated to estimate the ORC performance under Worldwide Harmonized Light Vehicles Test Cycle. Results show that ORC system can substantially alleviate the thermal damage caused by high exhaust temperature and extend TWC lifespan. It is estimated that over 98.5 % of thermal damage can be decreased by proper ORC setting, and the average TWC lifespan extension can be at least 55.4, making a reduced noble metal usage and cost of TWC. Meanwhile, with the decrease of the working temperature of TWC, ORC can recover exhaust energy under more road conditions, further improving the net power and shortening the payback period of extra ORC hardware costs. A reduction in the working temperature of TWC from 770.5 K to 618 K yields a 109 % enhancement in maximum power, coupled with a 62.30 % reduction in the payback period. These findings fully reflect the advantage of ORC-TWC coupling and indicate that ORC is supposed to be used more for the TWC with a low working temperature to maximize economic effectiveness. This study provides a novel pathway for thermal aging alleviation of TWC and a valuable reference for prospective studies on matching ORC with TWC under road conditions.

## 1. Introduction

Decarbonizing the transport sector requires cleaner fuels with less carbon footprint [1,2]. With the highest H/C ratio in fossil fuels, natural gas (NG) reduces $CO_2$ emissions by about 20 % compared to petrol and diesel, guaranteeing it is still a nonnegligible option for transport sector [3]. Lean-burn NG engines with selective catalytic reduction confront severe NOx penalties, especially in urban

* Corresponding author.
*E-mail address:* xin.wang@bit.edu.cn (X. Wang).

https://doi.org/10.1016/j.heliyon.2024.e33067
Received 2 November 2023; Received in revised form 2 June 2024; Accepted 13 June 2024
Available online 14 June 2024

driving [4]. To comply with the ever-tightening regulations, stoichiometric combustion combined with a three-way catalyst (TWC) is deemed more reliable, but at the price of high addition of precious metals to account for premature failure [5].

NG's high-temperature exhaust is the main reason causing the thermal aging of TWCs due to sintering and loss of active sites [6]. The extent of thermal aging increases with exhaust temperature and residual time [7]. Many studies have tried to extend the durability of engine after-treatment catalysts by changing the materials [8,9], structures [6,10], and production processes [11,12], but challenges persist [9].

Thermal aging can also be alleviated by mounting the TWC further away from the engine exhaust manifold. However, such an arrangement will slow down the catalyst light-off after engine cold-start, rendering emission homologation more difficult. Recent research on the organic Rankine cycle (ORC) waste heat recovery (WHR) [13], which utilizes the low-grade energy borne with exhaust, provides a new opportunity to improve the durability of the TWCs.

Previous ORC studies mainly focused on the energy conversion process and optimizing the factors affecting system efficiency and affordability, such as heat source, structure, working fluid, subassembly, and so on [14,15]. Studies on the ORC heat source indicate that stable and continuous engine waste heat is the conclusive factor affecting ORC performance [16,17]. Studies on the ORC structure indicate that engine waste heat can be maximally recovered by reasonably designing and optimizing the ORC structure [18,19]. Studies on the working fluid and main component indicate that the power output and thermal efficiency of the ORC can be efficiently improved by matching the optimum working fluid [20,21] and optimizing the subassembly, including the pump [22,23], evaporator [24,25], and expander [26]. These efficiency-oriented works are expected to absorb the waste heat borne with the exhaust as much as possible. However, this is not viable for modern vehicles because the emission after-treatment systems also require a warm atmosphere to operate properly.

Considering a balance between WHR and TWC conversion efficiency, Wang et al. proposed using an ORC system mounted between the engine exhaust manifold and TWC as an exhaust temperature chiller when the exhaust temperature was higher than $T_{90}$ (which corresponds to 90 % conversion efficiency) of the TWC [27]. An engine simulation result over the full engine map indicated that this method could significantly extend the lifespan of the TWC, and extra power could be recovered at moderate to high engine loads. Based on the same concept, this study further examines the potential benefits of enrolling an ORC system as an exhaust temperature chiller upstream of the TWC under real road conditions, with a certification drive cycles (namely, Worldwide Harmonized Light Vehicles Test Cycle (WLTC)) employed to represent the real traffic.

## 2. Methodology

This study is conducted via simulation. The NG engine simulation model is established by GT-Suite software and validated by experimental data. A vehicle dynamic model is established based on force analysis. These models are used to study the NG engine's exhaust waste heat under WLTC. Following this, the ORC net power output under WLTC is obtained based on the fitted function between exhaust waste heat and ORC power output reported in Ref. [27]. The thermal aging model of the TWC is established based on the Arrhenius equation, aimed at comparatively analyzing the accumulated thermal damage and the relative lifespan extension of the TWC under WLTC after the ORC intervenes.

### 2.1. Engine model

An NG engine is selected as the research object of this study, with the main technical parameters shown in Table 1. Before the engine model establishment, the reasonable assumptions benefit the simplification of the simulation, with the details found in Ref. [27].

The NG engine thermal system consists of the intake subsystem, injector subsystem, cylinder subsystem, crankshaft subsystem, and exhaust subsystem. The intake/exhaust subsystems mainly consist of some pipes and valves, which can be modeled by adopting "piperound", "flowsplitgeneral", and "valvecamconn" models. The cylinder subsystem focuses on the combustion and heat transfer of fuel, which can be established by adopting "EngCylCombSITurb" and "WoschniGT" models. The crankshaft subsystem is established by adopting the "EngineCranktrain" model which is widely used to simulate the common reciprocating internal combustion engine cranktrain configurations. The injector subsystem is established by adopting the "InjAF-RatioConn" model. The details and technical parameters for these models can be found in Ref. [27]. The engine model can be obtained by linking these subsystem models, shown in Fig. 1.

To ensure the engine model's accuracy, the experimental data of the brake torque, cylinder pressure, and exhaust temperature are

**Table 1**
The specifications of NG engine.

| Parameter | Value | Unit |
|---|---|---|
| Fuel | NG | / |
| Air-to-fuel ratio | 17.2 | / |
| Displacement | 1.012 | L |
| Rated power | 39 | kW |
| Maximum torque | 78 | N·m |
| Rated engine speed | 5300 | r/min |

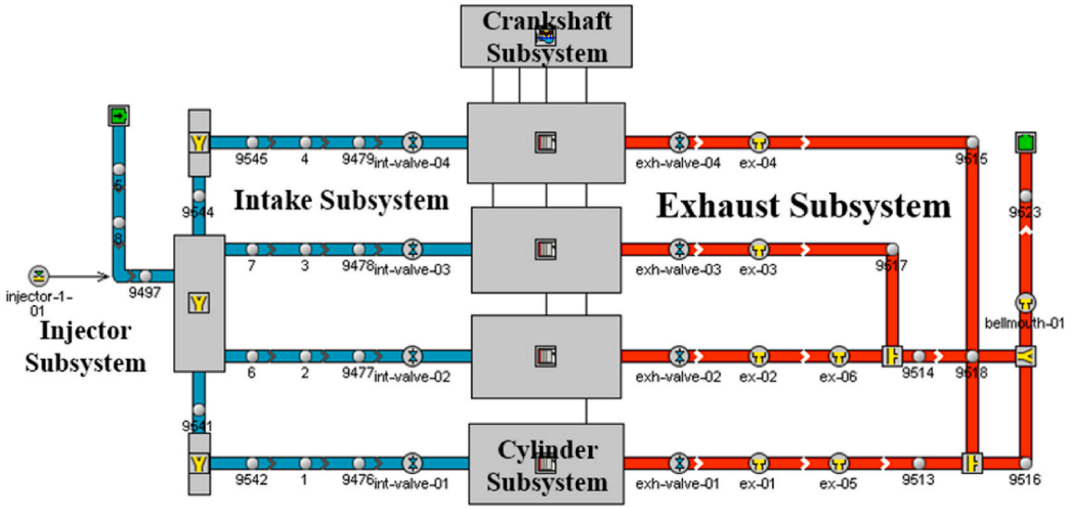


**Fig. 1.** NG engine model.

measured to compare with the simulation results, with the detailed measurement arrangement found in Ref. [27] and the comparison results shown in Fig. 2. For the engine brake torque, Fig. 2(a) and (b) show that small relative errors exist between the experimental data and the simulation results for both variations of brake torque with engine speed and throttle opening, with maximum relative errors of −2.98 % and 1.1 %, respectively. For the cylinder pressure, Fig. 2(c) shows that the simulation result is consistent with the experimental data, with a maximum relative error of the maximum cylinder pressure of 2.31 % and a deviation of the crank angle of 0.3 °CA. For the exhaust temperature, Fig. 2(d) shows ideal conformity between the experimental data and the simulation result at the moderate engine speed, with an absolute error of only a few Kelvin. Although the difference between the experimental data and the

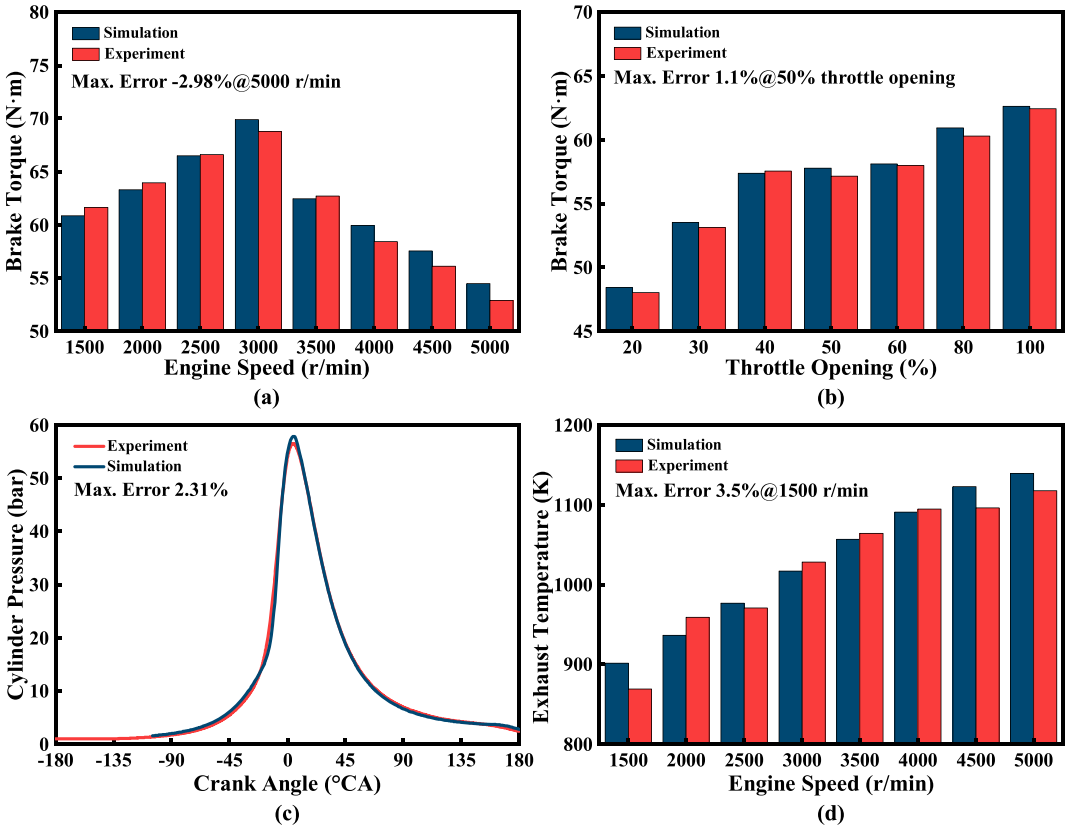


**Fig. 2.** Validated results of the engine model.

simulation results of exhaust temperature looks relatively high under low- and high-speed operating conditions, the maximum relative error is no more than 3.5 %. Therefore, all relative errors of these critical performance indexes mentioned above are within acceptable margins, indicating that the engine model is accurate and can be used for subsequent research.

### 2.2. Vehicle dynamic model

A light-duty commercial vehicle fueled with gasoline, compliant with China-IV standards, and used for short-range good transport is selected as the research object, with the main technical parameters shown in Table 2.

Based on force analysis for the vehicle, a simplified vehicle dynamic model is established, using the form of Formulas (1) to (7) [28]. These formulas are used to calculate the corresponding engine speed and brake torque according to all kinds of forces impacting the vehicle and vehicle velocity during the driving process. During the driving process of a vehicle, the total driving resistance of the vehicle includes rolling resistance, air resistance, climbing resistance, and acceleration resistance, which can be calculated using Formulas (1), (2), (3), and (4), respectively. Given the dynamic balance between the total driving force and the total driving resistance during the driving process, the total driving force can be calculated using Formula (5). The total driving force of the vehicle is derived from the engine and correlated with the engine brake torque; therefore, the engine brake torque can be calculated using Formula (6). Furthermore, the engine speed is mainly related to vehicle velocity, which can be calculated using Formula (7).

$$F_r = W \times f \tag{1}$$

Where $W$ represents the total loading imposed on the wheels, N; $f$ represents the rolling resistance coefficient.

$$F_w = \frac{C_D \times A \times u^2}{21.15} \tag{2}$$

Where $C_D$ represents the air resistance coefficient; A represents the frontal area, $m^2$; $u$ represents vehicle velocity, km/h.

$$F_i = m \times g \times \sin\alpha \tag{3}$$

where $m$ represents the mass of vehicle, kg; $g$ represents gravitational acceleration, $m/s^2$; $\alpha$ represents the degree of slope, °.

$$F_j = \delta \times m \times \frac{du}{dt} \tag{4}$$

Where $\delta$ represents the correction coefficient of rotating mass; m represents the vehicle's mass, kg; $\frac{du}{dt}$ represents the driving acceleration of the vehicle, $m/s^2$.

$$F_t = F_r + F_w + F_i + F_j \tag{5}$$

where $F_r$ represents the rolling resistance, N; $F_w$ represents the air resistance, N; $F_i$ represents the climbing resistance, N; $F_j$ represents acceleration resistance, N.

$$F_t = \frac{T_{tq} \times i_g \times i_0 \times \eta_T}{r} \tag{6}$$

Where $F_t$ represents the total driving force of vehicle, N; $T_{tq}$ represents the engine brake torque, N·m; $\eta_T$ represents the mechanical efficiency of the transmission system.

$$u = 0.377 \times \frac{r \times n}{i_g \times i_0} \tag{7}$$

Where $u$ represents vehicle velocity, km/h; $r$ represents the radius of the wheel, m; $n$ represents the engine speed, r/min; $i_g$ represents the transmission ratio of the gear's box; $i_0$ represents the transmission ratio of the final reduction drive.

**Table 2**
Main technical parameters of vehicle dynamic model.

| Parameter | Value | Unit |
|---|---|---|
| Displacement | 1.012 | L |
| Rated power | 39 | kW |
| Maximum torque | 78 | N·m |
| Rated engine speed | 5300 | r/min |
| Gear and transmission ratio | 1st, 2nd, 3rd, 4th, and 5th/4.11, 2.43, 1.66, 1.23, and 0.98 | / |
| Reference mass | 985 | kg |
| Length/width/height | 3860/1580/1900 | mm |

### 2.3. Thermal aging model

The TWC's thermal aging model is established using the Arrhenius equation [7,29], which has been detailedly introduced in our previous study [27]. A "relative TWC lifespan" concept which has been defined in Ref. [27] is subsequently used to quantify the TWC lifespan extension.

When ORC is coupled with TWC to adjust the temperature, the TWC inlet temperature is determined by the operating conditions of the engine and ORC. Nevertheless, the TWC inlet temperature should equal $T_{90}$ for methane conversion no matter how much exhaust energy is absorbed by ORC, aimed at assuring the TWC's high conversion efficiency [27]. Considering that there are different $T_{90}$ values for different TWCs, three applied scenarios are formulated on the basis of the reviewed $T_{90}$ values (from Refs. [30–41], with the details shown in Table S2 which can be found in the supplementary material) to estimate more comprehensively the feasibility of the ORC used to adjust temperature and recover exhaust energy.

(1) Conservative scenario: Aimed at old TWC technologies with relatively high working temperature, the ORC is mainly used as an exhaust cooler. Recovering the exhaust energy and decelerating the thermal aging give way to TWC's conversion efficiency, with the $T_{90}$ of 770.5 K.
(2) Balanced scenario: Aimed at current TWC technologies, recovering exhaust energy, extending the TWC lifespan, and securing efficient conversion of TWCs are equivalently important, with the $T_{90}$ of 698 K.
(3) Radical scenario: Aimed at the TWC technologies with the low working temperature, the ORC's function emphasizes recovering exhaust energy and extending the TWC lifespan. These intentions require a further reduction in temperature, with the $T_{90}$ of 618 K.

## 3. Results and discussion

The road condition directly determines the engine operating condition, further affecting the engine waste heat, ORC power output, and thermal aging of the TWC. Therefore, the engine exhaust waste heat, ORC performance, and TWC lifespan extension are studied under WLTC to study the feasibility of the ORC in recovering exhaust energy and extending the TWC lifespan under different road conditions.

As a transient road condition, WLTC is completed and more complicated than the New Europe Driving Cycle. It can simulate all kinds of real road conditions during the driving process. Therefore, WLTC is used for this study. Given the effect of road conditions on engine operating conditions, the variation of engine speed with time under WLTC is studied using the vehicle dynamic model, with the results shown in Fig. 3. Fig. 3 shows that the variation of engine speed with time is consistent with that of vehicle velocity. Under low-speed road conditions within 0–589 s, the engine speed is comprehensively low and fluctuates violently because of low vehicle velocity and frequent stop-starts of the vehicle. When the vehicle velocity is 20–40 km/h and 10–20 km/h, the corresponding engine speed is 2000–3000 r/min and 1500–2000 r/min, respectively. Under medium-speed road conditions within 590–1022 s, the engine speed relatively increases but fluctuates frequently because of the high vehicle velocity and few stop-starts. When the vehicle velocity remains in the 60–80 km/h range, the corresponding engine speed remains in the 2500–3000 r/min range. Under high-speed and extra high-speed road conditions within 1023–1800 s, the engine speed increases and fluctuates slightly within a small range because of the high and relatively stable vehicle velocity. The engine speed is 4000–4800 r/min when the vehicle velocity varies from 110 km/h to 130 km/h.

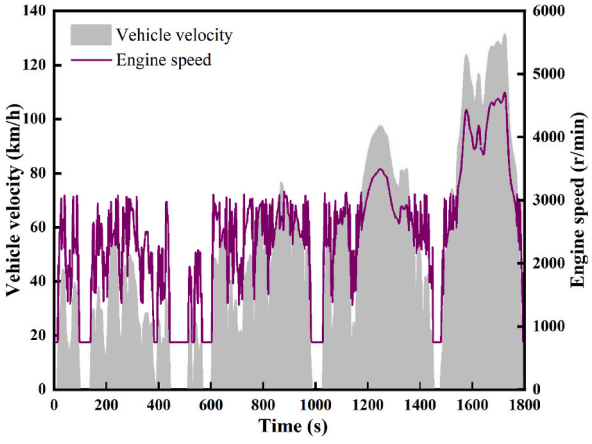


**Fig. 3.** Variation of engine speed and vehicle velocity with time.

### 3.1. Engine exhaust waste heat

The characteristics including the temperature and the mass flow rate of engine exhaust waste heat, not only severely affect the extent of TWC thermal aging but also directly determine the waste heat availability. Therefore, the variation of exhaust temperature and mass flow rate with time under WLTC is studied based on the engine model.

In Fig. 4, the exhaust temperature is very high and more than 800 K under most road conditions of WLTC, mainly because of the low flame speed of NG and the relatively poor effect of turbulent combustion. The trend of exhaust temperature is mainly related to engine speed. The exhaust temperature is relatively low and fluctuates violently under low and medium-speed road conditions, mainly ranging from 750 to 1000 K and an average of 835 K. Under high and extra high-speed road conditions, the exhaust temperature further increases and mainly ranges from 750 K to 1130 K, with an average of 973 K. Given that the working temperature ($T_{90}$) of most traditional TWCs is less than 800 K, the trend of this engine exhaust temperature indicates the necessity to adjust the temperature for the after-treatment system. Fig. 4 shows that the exhaust mass flow rate is low under WLTC, with a maximum of only 49 g/s and an average of 13 g/s, which is mainly attributed to this engine's small displacement and the gas engine's high air-to-fuel ratio.

Furthermore, past research has indicated that ORC could not yield the net power output when the exhaust energy is very small because the low exhaust energy cannot offset the friction between the assemblies to drive the expander, or the power yielded by the expander is too small to offset the power consumption from the pump [27,42]. Therefore, on the basis of the fitted function (shown in Formula (8)) between exhaust energy and net power output proposed by Ref. [27], the ORC's working status in this study is divided into exhaust cooler (ORC is only used to reduce exhaust temperature when the available exhaust energy does not exceed 5.77 kW) mode and combined mode (ORC is expected to yield net power output except reducing the temperature when the exhaust energy exceeds 5.77 kW). Last but not least, the ORC outlet temperature is required to be set to the $T_{90}$ of the TWC for the exhaust cooler mode and combined mode to achieve a good balance between TWC lifespan extension, exhaust energy recovery, and TWC's high conversion efficiency.

$$\dot{W}_{net} = -0.000002319 \cdot \dot{Q}_{exh}{}^{4} + 0.0001821 \cdot \dot{Q}_{exh}{}^{3} - 0.003171 \cdot \dot{Q}_{exh}{}^{2} + 0.05893 \cdot \dot{Q}_{exh} - 0.2671 \quad (8)$$

Where $\dot{W}_{net}$ is the ORC net power output, kW; $\dot{Q}_{exh}$ is available exhaust energy, kW.

### 3.2. Analysis of the ORC performance

This section details the ORC performance of recovering exhaust energy and extending TWC lifespan under WLTC. The sustainability of the ORC between the three applied scenarios is also compared.

#### 3.2.1. Conservative scenario

The ORC outlet temperature is set to 770.5 K in this scenario, which is mainly designed to estimate the ORC performance when matched with the old TWC technology before the Euro-5 regulation.

The available exhaust energy and the ORC net power output in the conservative scenario are calculated based on Formulas (9) and (8), as shown in Fig. 5. In Fig. 5, under low-, medium-, and even high-speed road conditions, the available exhaust energy and the ORC net power output are very small. No ORC net power output exists under more than half of the road conditions, and the maximum value

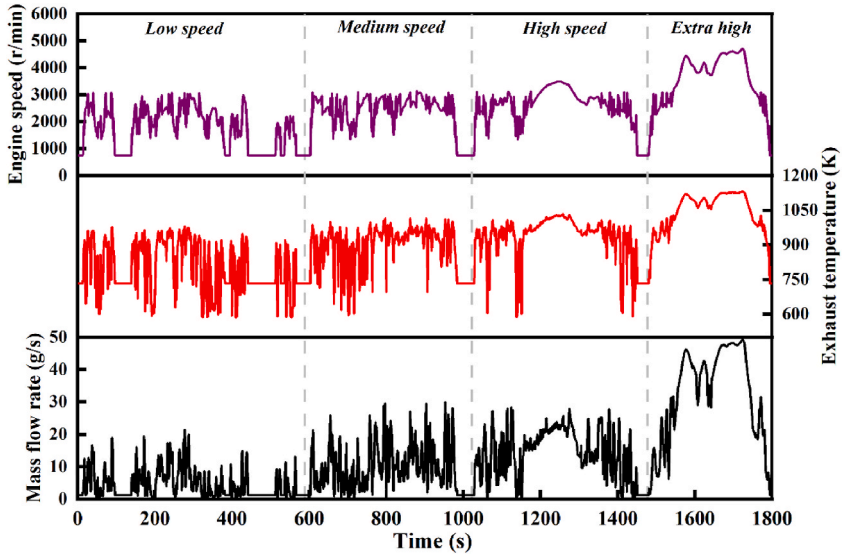


**Fig. 4.** Variation of the exhaust temperature and mass flow rate with time.

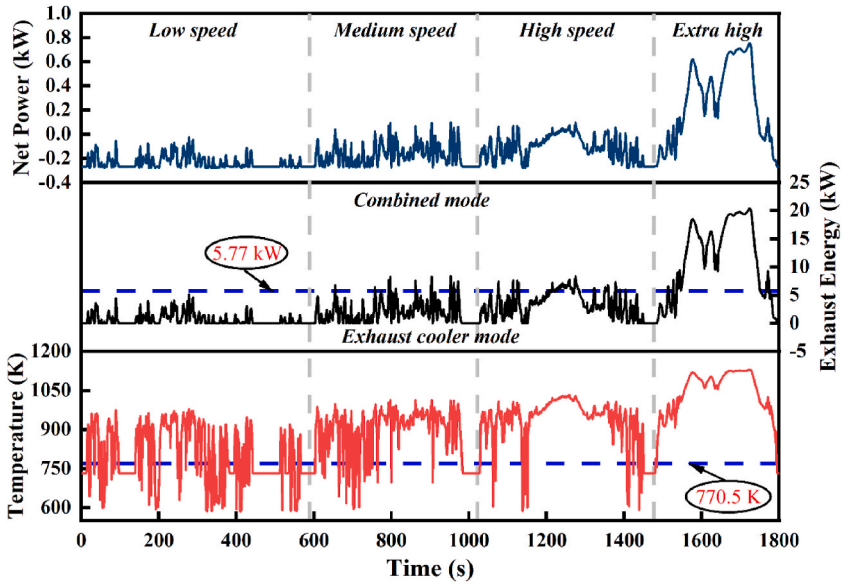


**Fig. 5.** Variation of the exhaust energy and ORC net power with time.

is not more than 0.1 kW under residual road conditions. This finding means the ORC is supposed to work in exhaust cooler mode under low-, medium-, and high-speed road conditions. The reasons for this phenomenon are as follows: (1) The exhaust temperature is less than 770.5 K under 30 % of road conditions, including low-, medium-, and high-speeds. This finding indicates that no available exhaust energy exists under these road conditions. (2) Although the exhaust temperature is more than 770.5 K under most residual road conditions, the available exhaust energy is smaller than 5.77 kW, which is not enough to drive the ORC to yield a positive power output. However, the available exhaust energy increases under extra high-speed road conditions, and the maximum ORC net power output reaches 0.75 kW. The ORC emphasizes adjusting the exhaust temperature when matched with the old TWC. However, the ORC can also yield nonnegligible net power when the engine speed is very high. This finding means that the ORC is likely to work in the combined mode under extra high-speed road conditions to cool the exhaust temperature while recovering exhaust energy.

$$\dot{Q}_{exh} = c \times \dot{m} \times (T_{exh} - T_{out}) \tag{9}$$

Where $\dot{Q}_{exh}$ is available exhaust energy, kW; $c$ is the specific heat capacity of exhaust, kJ/(kg·K); $\dot{m}$ is exhaust mass flow rate, kg/s; $T_{exh}$ is exhaust temperature, K; $T_{out}$ is ORC outlet temperature, K.

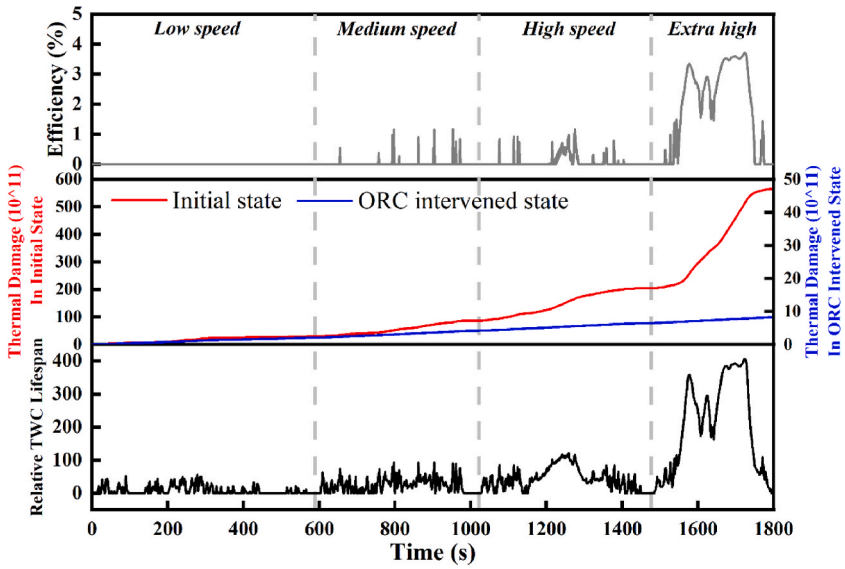


**Fig. 6.** Variation of the WHR efficiency, thermal damage, and relative TWC lifespan with time.

The ORC-WHR efficiency is calculated using Formula (10) to estimate the ORC performance in recovering exhaust waste heat. In Fig. 6, the maximum WHR efficiency is at most 1 % from low-speed to high-speed road conditions, most of which are zero because the available exhaust energy is very low under corresponding road conditions. As exhaust energy increases, the WHR efficiency starts increasing, and the maximum efficiency reaches 3.71 % under extra high-speed road conditions, with an average of 1.81 %. The thermal damage and the relative TWC lifespan are obtained based on the TWC thermal aging model to estimate the ORC performance in alleviating TWC thermal aging further. Fig. 6 shows that the accumulated rate of TWC thermal damage decreases after the ORC intervenes, particularly for extra high-speed road conditions because the ORC decreases the exhaust temperature under most road conditions. The total accumulated thermal damage of the TWC under the whole WLTC after the ORC intervenes decreases from 558.82 to 8.2, with a decrease of 98.5 %. Furthermore, the maximum relative TWC lifespan is 405.7 under WLTC, with an average of 55.4. The higher the engine speed is, the greater the relative TWC lifespan is. Because engine speed dominates exhaust temperature, and the relative TWC lifespan increases exponentially with exhaust temperature [27].

$$\eta_{ORC} = \frac{\dot{W}_{net}}{\dot{Q}_{exh}} \times 100\% \tag{10}$$

Where $\eta_{ORC}$ is the WHR efficiency; $\dot{W}_{net}$ is ORC net power output, kW; and $\dot{Q}_{exh}$ is available exhaust energy, kW.

### 3.2.2. Balanced scenario

The ORC outlet temperature is set to 698 K in this scenario, which is mainly designed to estimate the ORC performance when matched with the current TWC technology.

The available exhaust energy and the ORC net power output in a balanced scenario are calculated based on Formulas (9) and (8), as shown in Fig. 7. Fig. 7 shows that exhaust energy availability in the balanced scenario is higher than that of the conservative scenario because the ORC outlet temperature is lower in the balanced scenario. This finding means that many road conditions where ORC can theoretically recover exhaust energy exist. These conditions account for 93.84 % of road conditions and incorporate low, medium, and high speeds. However, the available exhaust energy is too low to drive the ORC to yield positive power, or the produced power is very small and not very stable under low- and medium-speed road conditions. Thus, the ORC is limited only to working in exhaust cooler mode under corresponding road conditions, to match efficiently with the current TWCs conforming to Euro-5 and Euro-6 or equivalent regulations. Under high road conditions, although the maximum ORC net power output is only 0.19 kW, a continuous positive power output exists under approximately 21.15 % of road conditions with the increase in available exhaust energy. Under extra high-speed road conditions, the ORC can continuously yield positive power except for the start and end stages. The maximum can reach 1.11 kW because of the high available exhaust energy. Therefore, when matched with the current TWC technology, the ORC can work efficiently in the combined mode under high and extra high-speed road conditions to adjust the exhaust temperature while recovering exhaust energy.

Fig. 8 shows the variation of the WHR efficiency with time. Under low- and medium-speed road conditions, the WHR efficiency is very small because of the low available exhaust energy. This finding further emphasizes that the ORC is only suited to adjust temperature under corresponding road conditions. The increased available exhaust energy improves the WHR efficiency to a different extent. The WHR efficiency is still small but stable under high-speed road conditions. It further increases under extra high-speed road

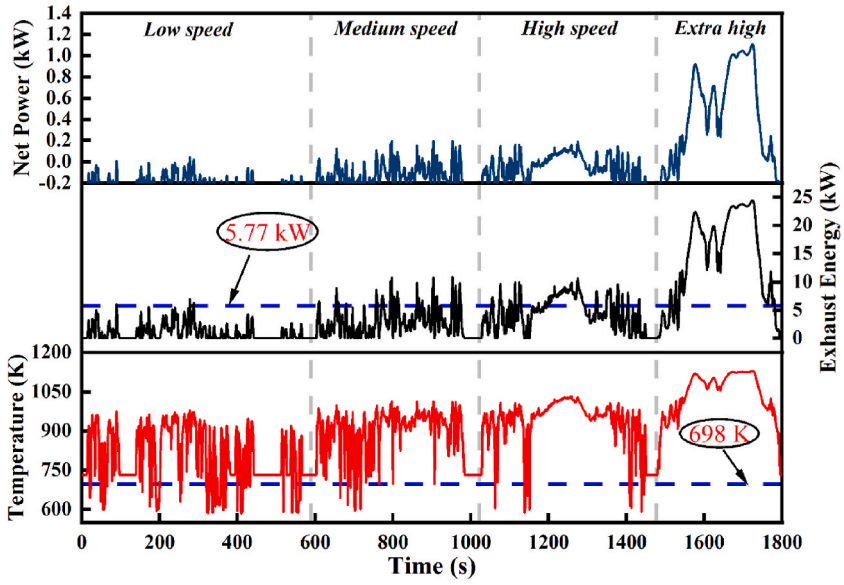


**Fig. 7.** Variation of the exhaust energy and ORC net power with time.

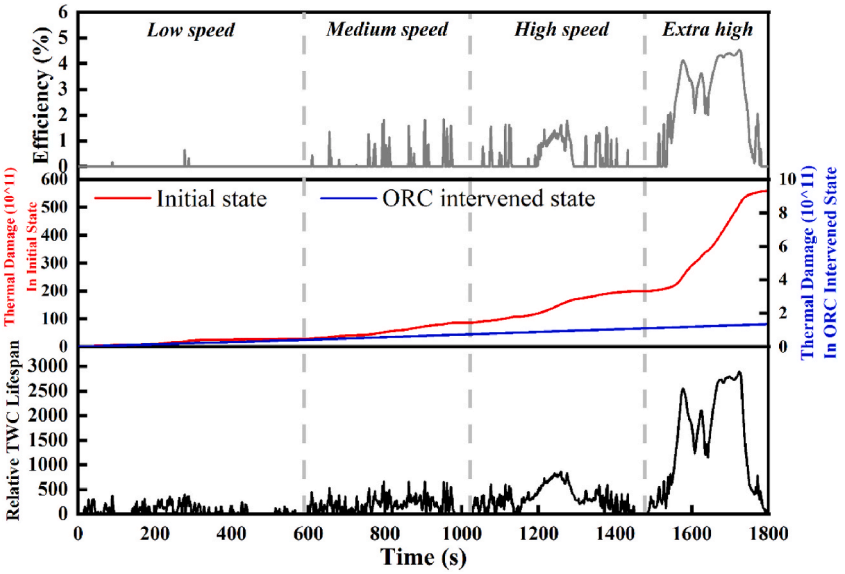


**Fig. 8.** Variation of the WHR efficiency, thermal damage, and relative TWC lifespan with time.

conditions, with a maximum reached 4.54 %. Furthermore, the relative TWC lifespan and the comparison of the TWC's accumulated thermal damage between the initial state and the ORC intervened state are shown in Fig. 8. Fig. 8 shows that the TWC's accumulated thermal damage is decreased by two orders of magnitude under the whole WLTC from 558.82 in the initial state to 1.35 in the ORC intervened state, with a decreased extent of 99.70 %. The relative TWC lifespan substantially increases as the accumulated thermal damage substantially decreases after the ORC intervenes. Under low- and medium-speed road conditions, the maximum relative TWC lifespan reaches 862, with an average of 173. Under high and extra high-speed road conditions, the maximum relative TWC lifespan can reach 2885.93, with an average of 1403. Therefore, when matched with the current TWC technology, the ORC can efficiently alleviate TWC thermal damage under low- and medium-speed road conditions, and the effectiveness of ORC in alleviating the thermal aging of the TWC will be more considerable under high- and extra high-speed road conditions.

### *3.2.3. Radical scenario*

The ORC outlet temperature is set to 618 K in this scenario, which is mainly designed to estimate the ORC performance when matched with the prospective TWC technology with an ideal low-temperature performance.

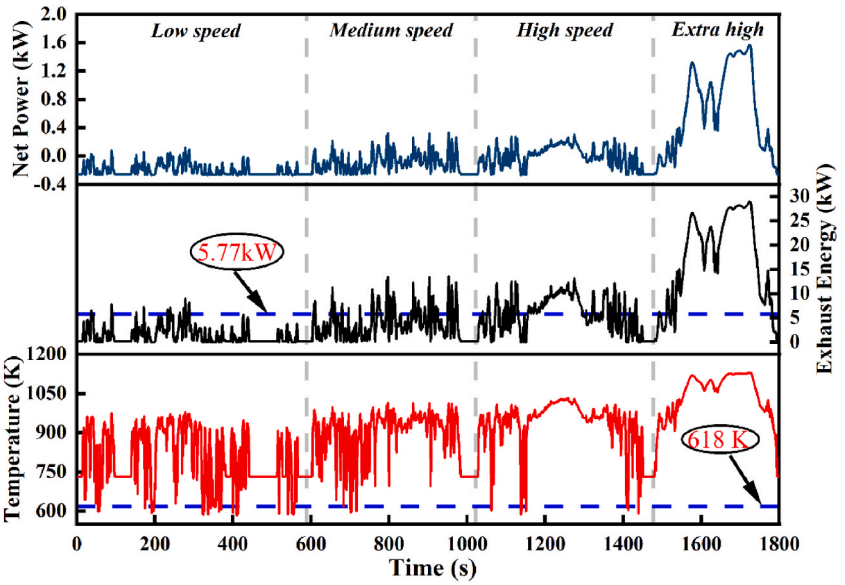


**Fig. 9.** Variation of the exhaust energy and ORC net power with time.

The available exhaust energy and the ORC net power output in the radical scenario are calculated based on Formulas (9) and (8), as shown in Fig. 9. Fig. 9 shows that the exhaust temperature under almost the whole WLTC can meet the corresponding requirement because of the low working temperature required by the prospective TWC technology. This observation means that exhaust energy is theoretically available under almost all road conditions. However, the bottom line of the available exhaust energy that drives the ORC to yield positive power is at least 5.77 kW. Thus, the ORC under low-speed road conditions cannot be used to recover exhaust energy because of low exhaust energy, and it can be used only to adjust the temperature. Although exhaust energy fluctuates violently under medium-speed road conditions, the available exhaust energy is more than 5.77 kW under 21.94 % of road conditions. The maximum ORC net power output reaches 0.33 kW under corresponding road conditions. This finding means that the ORC under medium-speed road conditions can be considered to switch the working mode from exhaust cooler mode to combined mode according to the actual requirement. Although the ORC net power output is still small under high-speed road conditions, the ORC can yield continuous positive power output under almost half of the road conditions. The ORC can yield a stably positive power output under extra high-speed road conditions, with a maximum of 1.57 kW. Therefore, when matched with the prospective TWC technology with a low working temperature, the ORC is allowed to work in the combined mode under high- and extra high-speed road conditions, can be switched to an alternative working mode under medium-speed road conditions, and is limited to working in exhaust cooler mode under low-speed road conditions.

Fig. 10 shows the variation of the WHR efficiency with time in the radical scenario. The WHR efficiency under medium- and high-speed road conditions is low, with a maximum of 2.40 %. Nevertheless, the efficiency fluctuation gradually decreases with the increase and stabilization of exhaust energy from medium-to high-speed road conditions. Under extra high-speed road conditions, the WHR efficiency can be continuously maintained at more than 3 % after start-up, and a maximum of 5.42 % can be reached. Furthermore, the comparison of the accumulated thermal damage of the TWC between the initial state and ORC intervened state and the relative TWC lifespan are shown in Fig. 10. Fig. 10 shows that the accumulated thermal damage of the TWC under the whole WLTC decreases by four orders of magnitude from 558.82 to 0.09 after the ORC intervenes. The substantial decrease in thermal damage is mainly attributed to the substantial adjustment in exhaust temperature. The temperature affects exponentially accumulated thermal damage, leading to an enormous relative TWC lifespan. Under low-speed road conditions where the ORC is only limited to working in exhaust cooler mode, the average and maximum relative TWC lifespan are 960 and 5976, respectively. Under residual road conditions where the ORC is allowed to work in the combined mode, the average and maximum relative TWC lifespan reach up to 8245 and 42904 because of the enormous temperature differences after the ORC intervenes. Therefore, when matched with the prospective TWC technology with a low working temperature, the ORC always has remarkable effectiveness in alleviating the thermal aging of TWC wherever any road conditions.

#### *3.2.4. Comparison of sustainability between three scenarios*

As shown in Table 3, the critical dynamic and economic indexes of ORC are compared between the three scenarios to study ORC sustainability further. The dynamic index mainly incorporates the maximum net power output and the WHR efficiency of the ORC, with the specific value from the analysis in Sections 3.2.1-3.2.3. The economic index in this study mainly refers to the payback period of the ORC, obtained based on the economic model widely used in previous studies [43–45]. The detailed construction of the economic model can be found in the supplementary material.

Table 3 shows that the ORC sustainability is improved from the conservative to the radical scenario. In the conservative scenario, the ORC's maximum net power output is only 0.75 kW because of the low available exhaust energy, with a maximum WHR efficiency of only 3.71 %. The increased available exhaust energy results in the ORC's maximum net power outputs of 1.11 kW in the balanced scenario and 1.57 kW in the radical scenario, with increases of 48 % and 109 %, respectively. The maximum WHR efficiencies of the ORC also increased to 4.54 % in the balanced scenario and 5.42 % in the radical scenario. With the improvement of ORC's dynamic performance, it can be applied to more road conditions to recover exhaust energy, and the ORC's payback period is manifestly shortened. In the conservative scenario, the payback period of ORC is more than 6 years, which is shortened by 40.80 % in the balanced scenario and 62.30 % in the radical scenario, respectively. This finding indicates that the economic effectiveness of ORC will be increasingly lucrative as the working temperature of TWC further decreases in the future. Furthermore, the huge benefit of ORC in alleviating the thermal aging of the TWC can be found in Table 3. The decrease in thermal damage is not less than 98.50 %, and the average relative TWC lifespan is at least 55.40 in the three scenarios, which means that the required quantity of the noble metal catalyst in the TWC coupled with ORC is substantially decreased compared with the case in which the ORC does not intervene. Given the high price of the noble metal, a decrease in the noble metal catalyst can result in considerable economic effectiveness.

## 4. Conclusion

This study emphasizes the function of ORC in reducing temperature. It proposes to insert an ORC between NG engines and its TWC through simulation to decelerate thermal aging and recover waste heat. First, the NG engine simulation model, the TWC thermal aging model, and the vehicle dynamic model are built and validated. According to the temperature characteristics of different TWCs, three scenarios representing old, current, and prospective TWC technologies are formulated to estimate the feasibility of alleviating thermal aging and recovering exhaust energy. Finally, the ORC performance and the TWC lifespan extension in three scenarios are studied under WLTC through the simulation model. The main conclusions are as follows.

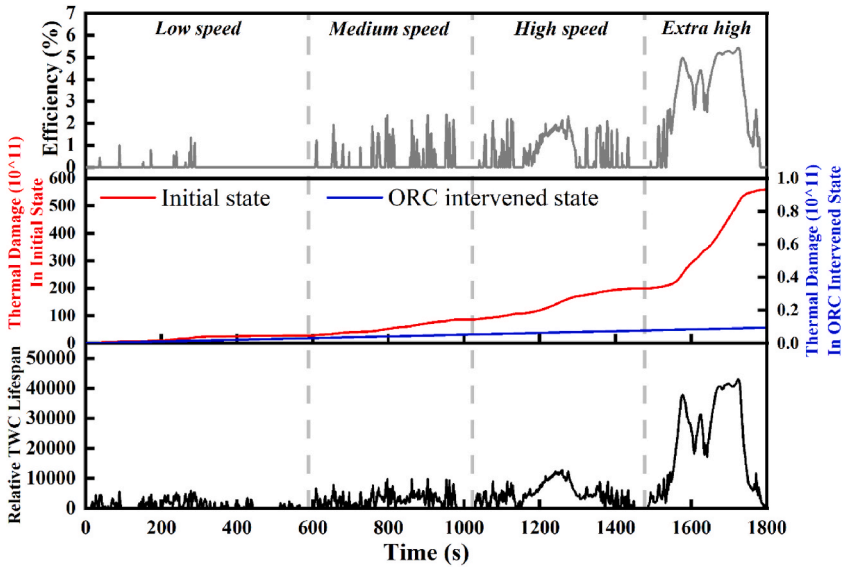


**Fig. 10.** Variation of the WHR efficiency, thermal damage, and relative TWC lifespan with time.

**Table 3**
Comparison of sustainability between the three scenarios.

| — | Conservative scenario | Balanced scenario | Radical scenario |
|---|---|---|---|
| Exhaust energy (kW) | 20.32 | 24.42 | 28.94 |
| Net power (kW) | 0.75 | 1.11 | 1.57 |
| WHR efficiency | 3.71 % | 4.54 % | 5.42 % |
| Operating mode | Combined/Cooling | Combined/Cooling | Combined/Cooling |
| Adaptable road condition | Extra high-speed/residual road conditions | Extra high- and high-speed/residual road conditions | Extra high-, high-, and medium-speed/low-speed road conditions |
| Payback period (year) | 6.87 | 3.93 | 2.59 |
| Decrease of thermal damage | 98.50 % | 99.70 % | four orders of magnitude |
| Average relative TWC lifespan | 55.40 | 173–1403 | 960–8245 |

(1) In the conservative scenario, ORC can yield net power output only under extra high-speed road conditions, with a maximum of 0.75 kW and a payback period of 6.87 years. Under other road conditions, the ORC is limited only to reducing the temperature, with a decrease in thermal damage of 98.50 % under WLTC and an average relative TWC lifespan of 55.40.
(2) In the balanced scenario, ORC can yield net power output under high and extra high-speed road conditions, with a maximum of 1.11 kW and the corresponding payback period of 3.93 years. However, under low- and medium-speed road conditions, the ORC is limited only to reducing the temperature, with a decrease in thermal damage of 99.70 % under WLTC and an average relative TWC lifespan of 173 under low- and medium-speed road conditions and 1403 under high- and extra high-speed road conditions.
(3) In the radical scenario, ORC can recover exhaust energy under all road conditions except low speed, with a maximum net power output of 1.57 kW and the corresponding payback period of 2.59 years. The decrease in thermal damage under WLTC can reach four orders of magnitude. Moreover, the average relative TWC lifespan can reach 960 under low-speed road conditions and 8245 under other road conditions.
(4) As the working temperature of the TWC decreases, the ORC exhibits an improved dynamic and economic performance and can be applied for more relatively low-speed road conditions, which provides a novel pathway for the alleviation of TWC thermal aging and a valuable reference for prospective studies on matching ORC with TWC under road conditions.

## Data availability statement

Data will be made available on request.

## CRediT authorship contribution statement

**Chongyao Wang:** Writing – original draft, Investigation, Formal analysis, Data curation, Conceptualization. **Xin Wang:** Resources,

Funding acquisition, Conceptualization. **Yunshan Ge:** Supervision. **Yonghong Xu:** Conceptualization. **Lijun Hao:** Software, Methodology. **Jianwei Tan:** Investigation, Formal analysis. **Ruonan Li:** Writing – review & editing. **Miao Wen:** Writing – review & editing. **Yachao Wang:** Validation.

## Declaration of competing interest

The authors declare that they have no known competing financial interests or personal relationships that could have appeared to influence the work reported in this paper.

## Acknowledgments

This work was supported by the National Natural Science Foundation of China (52272342) and National Key Research and Development Program of China (2022YFE0209000).

## Appendix A. Supplementary data

Supplementary data to this article can be found online at https://doi.org/10.1016/j.heliyon.2024.e33067.

## Nomenclature

| | |
|---|---|
| $F$ | resistance (N) |
| $W$ | total loading imposed on the wheels (kg) |
| $f$ | coefficient of rolling resistance |
| $C_D$ | air resistance coefficient |
| A | frontal area ($m^2$) |
| $u$ | vehicle velocity (km/h) |
| $m$ | mass of the vehicle (kg) |
| $g$ | gravitational acceleration ($m/s^2$) |
| T | brake torque (N·m) |
| $i$ | transmission ratio |
| $r$ | radius of wheel (m) |
| $n$ | engine speed (r/min) |
| c | specific heat capacity (kJ/(kg·K)) |
| $\dot{m}$ | mass flow rate (kg/s) |

*Greek letters*

| | |
|---|---|
| $\eta$ | efficiency (%) |
| $\delta$ | correction coefficient of rotating mass |
| $\alpha$ | degree of slope |

*Subscript*

| | |
|---|---|
| r | rolling resistance |
| w | air resistance |
| i | climbing resistance |
| j | acceleration resistance |
| tq | brake torque |
| r | refined TWC life |
| o | original TWC life |

*Acronyms*

| | |
|---|---|
| TWC | Three-way catalyst |
| ORC | organic Rankine cycle |
| WHR | waste heat recovery |
| WLTC | Worldwide Harmonized Light vehicles Test Cycle |

## References

[1] H.Y. Wang, C.W. Ji, C. Shi, et al., Multi-objective optimization of a hydrogen-fueled Wankel rotary engine based on machine learning and genetic algorithm, Energy 263 (2023) 125961.

[2] H.Y. Wang, C.W. Ji, D. Wang, et al., Investigation on the potential of using carbon-free ammonia and hydrogen in small-scaled Wankel rotary engines, Energy 283 (2023) 129166.
[3] X. Wang, C.Y. Wang, R.N. Li, et al., Tracing the regulated emissions of field-aged gasoline/natural gas bi-fuel taxis from new to 160000 km: deterioration and environmental implications, Fuel 362 (2024) 130863.
[4] B.Y. Wu, Z. Jia, Z.G. Li, et al., Different exhaust temperature management technologies for heavy-duty diesel engines with regard to thermal efficiency, Appl. Therm. Eng. 186 (2021) 116495.
[5] Y.D. Ren, D.M. Lou, P.Q. Tan, et al., Emission reduction characteristics of after-treatment system on natural gas engine: effects of platinum group metal loadings and ratios, J. Clean. Prod. 298 (2021) 126833.
[6] F. Guo, J.W. Li, Y.B. Zhang, et al., Enhanced stability and catalytic performance of active Rh sites on $Al_2O_3$ via atomic layer deposited $ZrO_2$, J. Phys. Chem. Lett. 13 (38) (2022) 8825–8832.
[7] J. Le Louvetel-Poilly, S. Balaji, F. Lafossas, Development of three-way catalyst aging model: application to real driving emission condition [C], SAE 24 (2019) 47.
[8] C.Y. Huang, W.P. Shan, Z.H. Lian, et al., Recent advances in three-way catalysts of natural gas vehicles, Catal. Sci. Technol. 10 (2020) 6407–6419.
[9] A.K. Datye, M. Votsmeier, Opportunities and challenges in the development of advanced materials for emission control catalysts, Nat. Mater. 20 (8) (2020) 1049–1059.
[10] X. Jiang, J. Fan, S.Y. Xiang, et al., Superior catalytic activity and high thermal durability of $MgAl_2O_4$ modified $Pt/Ce_{0.5}Zr_{0.5}O_2$ TWC, Appl. Surf. Sci. 578 (2021) 151915.
[11] L. Lan, S.H. Chen, H.M. Li, et al., Optimized synthesis of highly thermal stable $CeO_2$-$ZrO_2/Al_2O_3$ composite for improved Pd-only three-way catalyst, Mater. Des. 147 (2018) 191–199.
[12] L. Lan, X. Huang, W.Q. Zhou, et al., Development of a thermally stable Pt catalyst by redispersion between $CeO_2$ and $Al_2O_3$, RSC Adv. 11 (12) (2021) 7015–7024.
[13] J.S. Feng, X.N. Cheng, H.H. Wang, et al., Effect of flue gas outlet temperature in evaporator on thermal economic performance of organic Rankine cycle system for sinter waste heat recovery, J. Iron Steel Res. Int. 30 (2023) 2378–2390.
[14] J.S. Pereira, M. Santos, R. Mendes, et al., Thermal degradation assessment study of a direct vaporization ORC based micro-CHP system under close-to-real operating conditions, Appl. Therm. Eng. 14 (2022) 118878.
[15] C. Ononogbo, E.C. Nwosu, N.R. Nwakuba, et al., Opportunities of waste heat recovery from various sources: review of technologies and implementation, Heliyon 9 (2023) e13590.
[16] X.L. Yu, Y. Huang, Z. Li, et al., Characterization analysis of dynamic behavior of basic ORC under fluctuating heat source, Appl. Therm. Eng. 189 (2021) 116695.
[17] S. Broekaert, T. Grigoratos, D. Savvidis, et al., Assessment of waste heat recovery for heavy-duty vehicles during on-road operation, Appl. Therm. Eng. 191 (2021) 116891.
[18] A. Javanshir, N. Sarunac, Z. Razzaghpanah, et al., Thermodynamic analysis of a regenerative organic Rankine cycle using dry fluids, Appl. Therm. Eng. 123 (2017) 852–864.
[19] J. Li, Z. Yang, J. Shen, et al., Enhancement effects of adding internal heat exchanger on dual-pressure evaporation organic Rankine cycle, Energy 263 (2023) 126329.
[20] X.X. Zhang, Y.Y. Zhang, J.F. Wang, et al., Evaluation and selection of dry and isentropic working fluids based on their pump performance in small-scale organic Rankine cycle, Appl. Therm. Eng. 191 (2021) 116919.
[21] M.T. Wang, J. Zhang, H.W. Liu, Comparison of dual-pressure organic Rankine cycle using zeotropic mixtures, Appl. Therm. Eng. 204 (2022) 117996.
[22] Y.X. Yang, H.G. Zhang, Y.X. Xu, et al., Experimental study and performance analysis of a hydraulic diaphragm metering pump used in organic Rankine cycle system, Appl. Therm. Eng. 132 (2018) 605–612.
[23] Y.X. Yang, H.G. Zhang, X.Y. Xu, et al., Matching and operating characteristics of working fluid pumps with organic Rankine cycle system, Appl. Therm. Eng. 142 (2018) 622–631.
[24] G. Carraro, R. Pili, A. Lazzaretto, et al., Effect of the evaporator design parameters on the dynamic response of organic Rankine cycle units for waste heat recovery on heavy-duty vehicles, Appl. Therm. Eng. 198 (2021) 117496.
[25] J.W. Luo, P. Lu, K.H. Chen, et al., Experimental and simulation investigation on the heat exchangers in an ORC under various heat source/sink conditions, Energy 264 (2023) 126189.
[26] H.X. Wang, B. Lei, Y.T. Wu, Simulations on organic Rankine cycle with quasi two-stage expander under cross-seasonal ambient conditions, Appl. Therm. Eng. 222 (2023) 119939.
[27] C.Y. Wang, X. Wang, Y.S. Ge, et al., Alleviating the thermal aging of three-way catalyst applied to natural gas, Appl. Therm. Eng. 231 (2023) 120926.
[28] J. Liu, Y.S. Ge, X. Wang, et al., On-board measurement of particle numbers and their size, J. Environ. Sci. 57 (2017) 238–248.
[29] H. Ahari, J. Phillips, T. Pauly, Statistical approach to diesel aftertreatment accelerated aging performance correlation to in-use population, Emission Control Science and Technology 7 (2021) 79–90.
[30] A. Winkler, D. Ferri, H. Roland, Influence of aging effects on the conversion efficiency of automotive exhaust gas catalysts, Catal. Today 155 (2010) 140–146.
[31] H.F. Li, G.Z. Lu, D.S. Qiao, Catalytic methane combustion over $Co_3O_4/CeO_2$ composite oxides prepared by modified citrate sol-gel method, Catal. Lett. 141 (2011) 452–458.
[32] S.K. Matam, E.H. Otal, M.H. Aguirre, et al., Thermal and chemical aging of model three-way catalyst $Pd/Al_2O_3$ and its impact on the conversion of CNG vehicle exhaust, Catal. Today 184 (2012) 237–244.
[33] D. Bounechada, G. Groppi, P. Forzatti, et al., Enhanced methane conversion under periodic operation over a Pd/Rh based TWC in the exhausts from NGVs, Top. Catal. 56 (2013) 372–377.
[34] Y. Lu, K.A. Michalow, S.K. Matam, et al., Methane abatement under stoichiometric conditions on perovskite-supported palladium catalysts prepared by flame spray synthesis, Appl. Catal. B Environ. 144 (2014) 631–643.
[35] H.Y. Shang, Y. Wang, Y.J. Cui, et al., Catalytic performance of Pt-Rh/CeZrYLa+LaAl with stoichiometric natural gas vehicles emissions, Chin. J. Catal. 36 (2015) 290–298.
[36] J. Gong, D. Wang, J.H. Li, et al., Dynamic oxygen storage modeling in a three-way catalyst for natural gas engine: a dual-site and shrinking-core diffusion approach, Appl. Catal. B Environ. 203 (2016) 936–945.
[37] Xi YZ, Ottinger N, Liu ZG. Development of a Lab Reactor System for the Evaluation of Aftertreatment Catalysts for Stoichiometric Natural Gas Engines [C]. SAE 2017-01-0999.
[38] F. Davide, E. Martin, K. Oliver, Methane oxidation over a honeycomb Pd-only three-way catalyst under static and periodic operation, Appl. Catal. B Environ. 220 (2018) 67–77.
[39] G. Andreas, P. Josh, C. Maria, et al., PGM based catalysts for exhaust-gas after-treatment under typical diesel, gasoline and gas engine conditions with focus on methane and formaldehyde oxidation, Appl. Catal. B Environ. 265 (2020) 118571.
[40] G.C. Zhang, J.J. Chen, Y. Wu, et al., Pd supported on alumina modified by phosphate: highly phosphorus-resistant three-way catalyst for natural gas vehicles, J. Taiwan Inst. Chem. Eng. 115 (2020) 108–116.
[41] J. Gong, J. Pihl, D. Wang, et al., $O_2$ dosage as a descriptor of TWC performance under lean/rich dithering in stoichiometric natural gas engines, Catal. Today 360 (2021) 294–304.
[42] Rui Zhao, H.G. Zhang, S.S. Song, et al., Integrated simulation and control strategy of the diesel engine–organic Rankine cycle (ORC) combined system, Energy Convers. Manag. 156 (2018) 639–654.

[43] X. Ping, B.F. Yao, H.G. Zhang, et al., Thermodynamic, economic, and environmental analysis and multi-objective optimization of a dual loop organic Rankine cycle for CNG engine waste heat recovery, Appl. Therm. Eng. 193 (2021) 116980.
[44] X.X. Yang, F.B. Yang, F.F. Yang, Thermo-economic performance limit analysis of combined heat and power systems for optimal working fluid selections, Energy 272 (2023) 107241.
[45] J. Song, L. Ping, T. Jaime, et al., Thermo-economic optimization of organic Rankine cycle (ORC) systems for geothermal power generation: a comparative study of system configurations, Front. Energy Res. 8 (2020) 6.

## Further reading

[46] P.J. Eric, Air-source heat pump carbon footprints: HFC impacts and comparison to other heat sources, Energy Pol. 39 (2011) 1369–1381.